Carbohydrate Polymers 85 (2011) 457–464

Contents lists available at ScienceDirect

Carbohydrate Polymers

journal homepage: www.elsevier.com/locate/carbpol

# A new Density Functional Theory (DFT) based method for supporting the assignment of vibrational signatures of mannan and cellulose—Analysis of palm kernel cake hydrolysis by ATR-FT-IR spectroscopy as a case study

Søren Barsberg*, Anand R. Sanadi, Henning Jørgensen

*Forest & Landscape, Faculty of Life Sciences, University of Copenhagen, Rolighedsvej 23, DK-1958 Frederiksberg C, Denmark*

ARTICLE INFO

*Article history:*
Received 20 January 2011
Received in revised form 28 February 2011
Accepted 7 March 2011
Available online 15 March 2011

*Keywords:*
Cellulose
Mannan
FT-IR
DFT
Molecular modelling
Palm kernel

ABSTRACT

Attenuated Total Reflectance (ATR) FT-IR spectroscopy gives *in situ* information on molecular concentration, organization and interactions in plant cell walls. We demonstrate its potential for further developments by a case study which combines ATR-FT-IR spectroscopy with a recently published DFT method for polysaccharide IR band assignments.

Palm kernel cake is enzymatically hydrolyzed and fermented, which targets cellulose and mannan in particular. The DFT method helps to identify their spectral changes and gives new knowledge on their spectral signatures. This method thus provides a *prerequisite* for FT-IR analysis. The removal of mannan is identified and correlates with positional shifts of both the mannan glycosidic linkage vibration at 1180 $cm^{-1}$ and the 896 $cm^{-1}$ cellulose exocyclic $C6H_2$ vibration. This indicates a cellulose environment change, and for mannan the theoretical results show a decreasing degree of polymerization to be a plausible cause, although others may interfere.



## 1. Introduction

Methods of obtaining knowledge on the chemical components of plant biomass, e.g. cellulose, lignin, hemicelluloses, are gaining importance with the increasing use of such materials as sources of energy and chemicals. The enzymatic or chemical catalyzed degradation of cell wall components for the production of low molecular weight compounds depends thus on the quantity and organization of these components. Chemical analysis methods typically employ reactions where cell wall material is degraded to its constituent components, e.g. monomeric sugars. Many factors of uncertainty are associated with such reactions, e.g. unwanted side-reactions, completion and yield, problems of recovery and subsequent analysis of reaction products. But more important, information about the nature and organization of cell wall macromolecules is inevitably destroyed. For example the detection of both mannose and glucose in a hydrolysate cannot help to elucidate whether these sugars originated from cellulose and mannan or from glucomannan polymer. This detailed macromolecular organization within the cell wall is in principle revealed by vibrational bands, e.g. by the infrared spectrum of the original biomass sample.

When infrared (IR) spectroscopy is combined with Attenuated Total Reflectance (ATR) a versatile and robust analysis method is obtained. It requires practically no sample preparation and reveals fundamental information on a diverse set of sample types, from proteins and organics in solution to polymers and wood surfaces (da Luz, 2006; Huang et al., 2010; Kaparaju & Felby, 2010; Kirov & Assender, 2005; Lin & Li, 2010; Oberg & Fink, 1998). Thus the molecular components of the sample and their *in situ* organization are preserved, and the information is obtained directly without intervening reaction and recovery steps. A specific advantage is that there is no limitation of sample thickness, and the sample is not required to be finely ground and dispersed in, e.g. a KBr tablet as for transmission spectroscopy.

The usually high (>$10^4$) signal-to-noise, which can be obtained by a research grade FT-IR spectrometer within a few minutes of acquisition time, counteracts to some degree a disadvantage of the method, i.e. the occurrence of multiple overlapping bands from different types of components in the spectrum of complex biomass materials. A second potential problem is that the ATR-IR spectrum is not trivially related to the absorption coefficient of the sample but is affected by, e.g. dispersion and wave number dependency of the penetration depth of the electromagnetic field (Goormaghtigh, Raussens, & Ruysschaert, 1999). However, for plant biomass and an appropriate ATR crystal material the recorded spectra are in the fingerprint region ~600–1800 $cm^{-1}$ in practice similar to conventional transmission spectra in respect to band positions and

* Corresponding author. Tel.: +45 3533 1500; fax: +45 3533 1508.
*E-mail addresses:* sbar@life.ku.dk (S. Barsberg), ansr@life.ku.dk (A.R. Sanadi), hnj@life.ku.dk (H. Jørgensen).

0144-8617/$ – see front matter © 2011 Elsevier Ltd. All rights reserved.
doi:10.1016/j.carbpol.2011.03.012

qualitative intensities, and correction procedures can if necessary improve this.

Band positions and intensities give information on the chemical composition and its possible changes. They also report on the *in situ* interactions between cell wall polymers and their environment, e.g. hydration effects. The use of known reference materials and/or tables of characteristic bands of chemical groups, or published information, can help interpret the observations. However, in some cases and especially for complex biomass samples the available information can be insufficient or has no sound justification. Thus a characteristic $\beta(1\rightarrow4)$ mannan IR band at $\sim$810–820 $cm^{-1}$ is often mentioned but the justification for its assignment is unclear (Joo & Yun, 2005; Kath & Kulicke, 1999; Yu, Jiang, Zou, Duan, & Xiong, 2009). The assignment of vibrational bands is significantly strengthened when it is based on electronic structure theory prediction of vibrations of appropriate models systems. Density Functional Theory (DFT), and its incorporation in software packages together with methods of solving for the vibrational modes and their intensities, has in conjunction with hardware efficiency seen tremendous development the last two decades.

In the present work we demonstrate the synergy between a practical application of ATR-FT-IR spectroscopy and DFT based prediction of vibrational properties of molecular model systems. Specifically we studied the *in vitro* enzymatic degradation of palm kernel cake (PKC) and then predicted and identified the characteristic bands of the presumed main molecular components, i.e. cellulose and mannan, which are targeted by the enzymatic treatment. Thus only the (unsubstituted) homopolysaccharides are considered here.

PKC is a potentially important resource for biorefining and is obtained as the residue after pressing out oil from the palm kernel. World annual production of palm oil for the period March 2008–2009 exceeded 43 million metric tons (USDA Foreign Agricultural Service, 2009). Palm oil is one of the largest sources of cooking oil in the world (Palm Oil World, 2009). Furthermore, there has been increasing interest in the use of the oil as a source of biofuels. Based on the production of palm oil, it can be estimated that around 4.5 million tons of PKC is available. Currently PKC is mainly used as a low efficiency animal feed limited by large fiber content and low nutritive source (Berepubo, Mepba, Agboola, & Onianwah, 1995; O'Mara, Mulligan, Cronin, Rath, & Caffrey, 1999; Ramachandran, Singh, Larroche, Soccol, & Pandey, 2007; Sundu, Kumar, & Dingle, 2006). In order to maximize the use and revenue of PKC, bioethanol can be produced by enzymatic hydrolysis of carbohydrates in PKC, and subsequent fermentation of the sugars into ethanol (Jørgensen et al., 2009). The carbohydrates consist predominantly of mannan and cellulose (Düsterhöft, Bonte, & Voragen, 1993; Düsterhöft, Posthumus, & Voragen, 1992; Knudsen, 1997). The linear form of mannan with a $(1\rightarrow4)$ linked β-D-mannopyranose backbone dominates with minor amounts (12–20%) of $(1\rightarrow6)$ linked α-D-galactopyranose (galactose) substitution (Aspinall, 1970; Düsterhöft et al., 1992; Sundu et al., 2006). The linearity results as for cellulose in a predominantly crystalline structure depending on degree of substitution. In addition small amounts of (4-O-methyl)glucuronoxylans and arabinoxylans are also found.

The enzymatic hydrolysis and fermentation of PKC provides a case study where the compositional change of the remaining PKC material can be monitored by ATR-IR spectroscopy. The present work shows that the original single component polymeric forms, e.g. mannan and cellulose, can be identified in pure forms. Several reference works can help identify the IR bands caused by cellulose. For mannan the study and assignments of its IR spectrum is significantly less developed, and the use of DFT for this purpose can thus prove its strength. For glucomannan (or any other hetero-polysaccharide) the situation is far more complex. The mannose/glucose content ratio can vary from $\sim$0 (cellulose) to $\infty$ (mannan) and for a given ratio the mannose and glucose units can be distributed in a *vast* number of ways increasing with the degree of polymerization. Well-defined experimental samples will to say the least be a challenge to obtain. In addition the theoretical modelling is faced with the principal necessity of fully exploring the conformational degrees of freedom (to identify low energy conformers), which for cellulose or mannan fortunately are restricted by their characteristic hydrogen bonding networks. An exploration concerning glucomannan is therefore not considered in the present work. The aim is to provide a *prerequisite* for FT-IR analysis of biomass samples, e.g. sugar composition, namely identification and assignment of spectral signatures from the PKC main polysaccharide constituents.

We show how the characteristic mannan and cellulose IR bands can be predicted from an $n\rightarrow\infty$ extrapolation procedure using $\beta(1\rightarrow4)$ mannan or cellulose chain models of *finite* degree of polymerization, $n=2$–5, of the pyranose unit. These predictions are compared with spectra of pure cellulose, mannan and the PKC hydrolysis system, and allow the assignment of several cellulose or mannan "fingerprint" bands. It is shown that second derivative spectra resolve overlapping bands of PKC. This allows a more informed FT-IR study of the impact of enzymatic hydrolysis on the PKC chemical state, and the origin of close lying bands in the spectra is resolved from a combined theoretical and experimental point of view.

## 2. Materials

PKC was supplied from P.T. Musim Mas, Indonesia, batch BS 2008-00031. The dry matter (DM) content was around 96%. The material was sieved through a 1 mm aperture mesh and the remainder ground using a Braun coffee grinder for 10 s and again sieved. This was repeated twice. Material that did not pass the mesh after the third grinding was discarded (Jørgensen et al., 2009). Microcrystalline cellulose (from Merck), Whatman No. 1 filterpaper (cellulose) and 1,4-β-D-mannan (Ivory nut, purity >98%, from Megazymes) were used as reference materials. The applied enzyme preparation consisted of monocomponent endo-mannanase, monocomponent β-mannosidase and a cellulase preparation (from Novozymes A/S, Bagsværd, Denmark). The ratio of endo-mannanase:β-mannosidase:cellulase was 53:12:1 and the total enzyme loading was 98.6 mL per kg of dry PKC. The β-mannosidase and cellulose preparations contained additional α-galactosidase and β-glucosidase activities. Details about the activities of the components in the enzyme mixture can be found elsewhere (Jørgensen et al., 2009).

## 3. Methods

The carbohydrate and lignin composition of the PKC material was measured using the strong acid hydrolysis process developed by Sluiter et al. (2006). Protein content was determined by the Kjeldahl method using a nitrogen factor of 6.25. The material was dried at 45 °C for 72 h prior to protein analysis.

### 3.1. PKC hydrolysis and fermentation

The enzyme mixture was used to pre-hydrolyze the PKC in a 100 mL polyethylene bottle placed in a rotating drum at 50 °C for 24 h as described in detail by Kristensen, Felby, and Jørgensen (2009). The experiment was performed with 50 g total mass in the bottles at 35% DM in 50 mM sodium citrate buffer (pH 4.8). After pre-hydrolysis the bottle was removed from the drum, and dry bakers yeast (*Saccharomyces cerevisiae*) from the supermarket

(Malteserkors, Lallemand, Denmark) was added corresponding to 7 g dry yeast per kg of initial DM. A needle was pierced and left on the bottle cap for the venting of carbon dioxide. The bottles were then placed in an Ecotron incubator shaker for simultaneous saccharification and fermentation (SSF) at 32 °C for 168 h at 180 rpm. Samples were taken after pre-hydrolysis and after SSF.

### 3.2. Sugar analysis

Separation and quantification of arabinose, galactose, glucose, mannose and xylose were done using a Dionex BioLC system with a CarboPac PA1 column (4 mm × 250 mm) and pulsed amperometric detection. The separation was performed at 25 °C using gradient elution with KOH at 1.05 mL/min and the following profile: 0–30 min 2 mM KOH, 30–35 min linear increase from 2 to 25 mM, 35–40 min 25 mM, 40–50 min 2 mM. Samples were appropriately diluted in MQ-water and filtered through a 0.2 μm filter prior to analysis.

The amount of ethanol was measured using a Dionex Summit HPLC system with a Phenomenex Rezex RHM column and a Shimadzu refractive index detector. Separation was performed at 80 °C with a flow rate of 0.6 mL/min of 5 mM $H_2SO_4$.

The solid fractions remaining after the pre-hydrolysis and SSF step, which we refer to as the H and HSSF fractions, respectively, were isolated by removing the supernatant after centrifugation and rinsing the remaining material three times with MilliQ water. These fractions were then dried at 45 °C for a week. The three types of samples, i.e. original PKC sample and the H and HSSF fractions, were evaluated with ATR-IR spectroscopy.

### 3.3. ATR-IR spectroscopy

Spectra were obtained by a Nicolet 6700 FT-IR spectrometer equipped with a temperature adjustable ATR (Golden Gate) unit and purged with dry air. All spectra were obtained as 100 scans at 4 $cm^{-1}$ resolution. The ATR crystal (single reflection diamond) and sample was maintained at $T = 30$ °C. The results are based on ten spectra of the original (non-modified) PKC sample and five spectra of the H and HSSF samples. Different portions of sample were always used for acquiring spectra.

Three spectra of different portions of the three reference materials were obtained using the same settings.

The influence of dispersion effects on the IR band positions was assessed for the reference materials by applying the advanced ATR correction in the spectrometer Omnic software. The required inputs were the diamond crystal and sample refractive indexes and the angle of incidence = 45°. This corrects both for wavelength dependence of the penetration depth of the EM field and for dispersion induced frequency shifts of band positions.

### 3.4. Prediction of IR bands

The Gaussian 03W (Rev. D.01) and Gaussview 3.0 software were used for the calculations and for building molecular models and analyzing results (Gaussian 03W, 2004). In short, a single cellulose or mannan chain was constructed such that the dihedral angles of the β(1 → 4) linkage, exocyclic MeOH and pyranose ring OH groups all reflected those of the crystal structures. For cellulose atomic coordinates were adopted from the Iβ crystal structure (Nishiyama, Langan, & Chanzy, 2002). For mannan the (heavy) atom coordinates defined only the glycosidic linkage conformation and one of the two MeOH dihedral angles (Chanzy, Perez, Miller, Paradossi, & Winter, 1987). The remaining dihedral angles, i.e. OH torsional states, were adopted from a molecular mechanics force field model of a mannan crystal (Yui, Miyawaki, Yada, & Ogawa, 1997).

The oligomeric models were then built to consist of either two, three, four or five β(1 → 4) linked pyranose units, which at the terminal 1 and 4 positions were substituted with an OMe group to mimic the continuation of a glycosidic linkage. All model chains were fully geometry optimized using the B3LYP functional and the pc-1 basis set with the p function removed from all hydrogens. Each final structure was subjected to B3LYP harmonic frequencies calculation (using the same basis set) to provide vibrational frequencies and IR intensities. These results confirmed all structures as true local energy minima. For more details on this computational method and assignment of IR bands the reader is referred to a recent publication (Barsberg, 2010).

The merit of this method is primarily the prediction of band positions (frequencies) and associated qualitative intensities. The calculated intensities cannot be expected to be of sufficient quality to be used on a quantitative basis. There are two primary reasons for this. First, the basis set is for practical reasons of limited size and does not include diffuse functions, which are required for quantitative results, and second, the coupling between single chains in the crystal – which the method does not account for – may be expected to affect the intensities (change of dipole moments) much more than the frequencies.

## 4. Results

In the following the advanced ATR correction for dispersion, etc. is demonstrated for a cellulose sample. Next we present the observed and DFT predicted mannan and cellulose IR band signatures. This forms a necessary basis for interpreting ATR-IR spectra of the PKC samples. Before these spectra are presented the results of the complementing sugar analysis of the PKC sample will be shown. It is then shown how the enzyme catalyzed polysaccharide degradation is reflected by changes in the ATR-IR spectra of the solid phases, i.e. the original PKC material compared with the solid residues obtained after pre-hydrolysis, H, and after the additional SSF step, HSSF.

### 4.1. ATR-IR spectra of reference samples

The three spectra of each reference sample type were practically identical with band position differences <0.5 $cm^{-1}$. Hence all results refer to the average spectrum. The two types of cellulose samples are identical except for a couple of weak bands which can differ in strength.

The influence of the ATR correction on the averaged spectrum of microcrystalline cellulose is seen in Fig. 1. The spectral shape is most affected in the strong absorption region around 1000 $cm^{-1}$ and is not sensitive to the choice of cellulose refractive index $n$ within the 1.4–1.6 range, where the corrected spectra mainly differ by a multiplicative factor. For both mannan and cellulose $n$ were set to $n = 1.46$. This is the value for cellulose extrapolated to the mid-IR range by fitting a simple exponential decay to the dispersion curve ($n$ as function of wavelength) in the optical range 400–1100 nm (Kasarova, Sultanova, Ivanov, & Nikolov, 2007). The effect of the correction on IR band positions as determined from the second derivative of the spectra (in the following abbreviated as *2der spectra*) was small, see Table 1. Thus the *largest* deviation is a 3 $cm^{-1}$ shift of the very strong (uncorrected) 1055 $cm^{-1}$ cellulose band.

In the lower half of Fig. 2 the mannan and MC cellulose reference sample spectra are depicted together with their 2der spectra, which have been sign-inverted and scaled by a multiplicative constant to ease the comparisons.

Above the 500–600 $cm^{-1}$ region, where 2der spectra are dominated by noise, very distinct spectral features are identified for both samples. Since these are summarized in Table 1 we point out

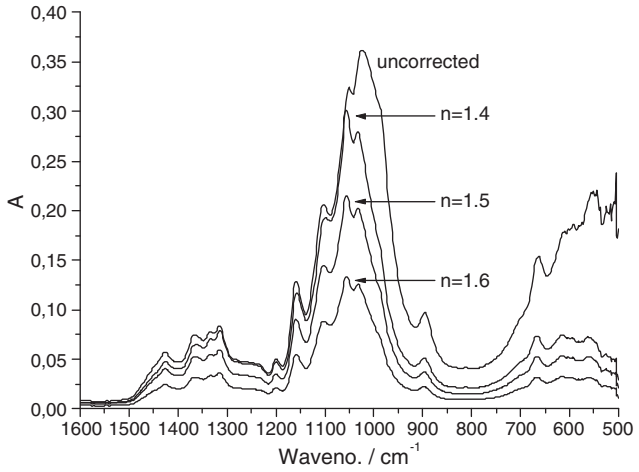


**Fig. 1.** ATR-FT-IR spectra of microcrystalline cellulose. The spectra displayed are (from the top): uncorrected spectrum, corrected spectrum using refractive index $n = 1.4$, $n = 1.5$ and $n = 1.6$, respectively.

here just the most marked ones. In the 650–700 $cm^{-1}$ interval a doublet band, which is resolved in the 2der spectrum, is found for cellulose. A corresponding weaker band, which is not resolved in the 2der spectrum, is found for mannan at a slightly lower position 641 $cm^{-1}$.

Whereas cellulose has no distinct bands in the ~700–900 $cm^{-1}$ interval, mannan has two dominant narrow bands in this interval, in addition to three weaker and also distinct bands. Another narrow mannan band is also located at 939 $cm^{-1}$ a position well separated from cellulose bands. The 1000–1150 $cm^{-1}$ interval is for both samples the most absorbing, but here it is difficult to separate cellulose and mannan bands as a large degree of overlap occurs. The characteristic 1161 $cm^{-1}$ (for cellulose) and 1180 $cm^{-1}$ (for mannan) bands distinguish these two types of polysaccharides. Except for a medium strength band at 1240 $cm^{-1}$, which due to its strength is characteristic for mannan, the 1200–1500 $cm^{-1}$ interval contains only weak features, which are not very distinct for either material. Thus mannan is most clearly distinguished from cellulose by its IR spectral fingerprints found in the 700–1000 $cm^{-1}$ interval. The molecular vibrational nature of these will be discussed below, and it will be shown how the PKC hydrolysis is directly monitored by these bands.

### 4.2. Simulated spectrum of mannan and cellulose

In a previous work the assignment of cellulose IR bands was supported by DFT predictions based on single cellulose chains, which reproduced band positions to an average error of ~10 $cm^{-1}$ (Barsberg, 2010). The two hydrogen bond networks A and B (NWA and NWB), which were modelled, gave very similar band positions and strengths within the 800–1500 $cm^{-1}$ range. Intermolecular interactions within the crystallites lead to relatively small perturbations of the peak positions within this range. In the present work the same method was also used for mannan models, and predicted incremental IR spectra of both polysaccharides (for cellulose only NWA is shown) are depicted in Fig. 2 above their corrected ATR-IR spectra.

The wave number axis of the predicted IR spectra was scaled to optimize the correspondence between well defined observed and predicted band positions in the 800–1200 $cm^{-1}$ interval. For cellulose six bands and for mannan nine bands were used. The optimal linear fit $\upsilon_{OBS} = f\upsilon_{CALC}$ resulted in a scaling constant $f = 0.983$ for both the cellulose and mannan band positions with an average absolute error of 9 and 8 $cm^{-1}$, respectively.

In Table 1 a summary is given of the correspondence and assignment of characteristic IR bands.

The simple change of all glucopyranose to mannopyranose residues (or *vice versa*) within the polysaccharide chain imparts significant qualitative changes to the IR spectrum and the predictions reflect this very well within the 800–1500 $cm^{-1}$ interval.

In the lower wave number part of the spectrum the cellulose 896 $cm^{-1}$ band distinguishes cellulose from mannan, which has a relatively weak band at 892 $cm^{-1}$ as is also reflected by the predictions. Mannan has, however, three characteristic fingerprint bands at 805, 871 and 939 $cm^{-1}$, and two weak bands positioned in the interval 750–800 $cm^{-1}$.

These relatively large differences between cellulose and mannan are reflected by the qualitative vibrational assignments, see Table 1. Thus many mannan bands, especially the three fingerprint

**Table 1**
ATR-corrected IR (2der) band frequencies (in $cm^{-1}$) and approximate strengths for cellulose and mannan assigned to their predicted band positions.

| Cellulose | Strength | Predicted unscaled | Predicted scaled | Assignment |
|---|---|---|---|---|
| 1161 | S | 1193 | 1173 | L υCO asym |
| 1110 | S | 1123 | 1104 | R OH groups υCO sym |
| 1057 | VS | 1067 | 1049 | L υC4O, MeOH υCO |
| 1032 | S | 1042 | 1024 | υC3O R υCC, υCO, L υCO sym, MeOH υCO |
| 983 | S | 1009 | 992 | R υCO, δ(C2)OH |
| 896 | M | 923 | 907 | MeOH $\delta CH_2$ |
| **Mannan** | **Strength** | **Predicted unscaled** | **Predicted scaled** | **Assignment** |
| 1180 | S | 1185 | 1165 | L υCO asym |
| 1141 | M | 1158 | 1138 | υC2O δ(C3)OH |
| 1125 | M | 1139 | 1120 | MeOH $\delta CH_2$, R υCC, υCO |
| 1113 | M | – | – | – |
| 1088 | M | – | – | – |
| 1077 | W | – | – | – |
| 1066 | S | 1083 | 1065 | R υCC, υCO asym, MeOH υCO |
| 1033 | M | 1066 | 1048 | L υC4O, MeOH υCO |
| 1011 | S | 1042 | 1024 | υC3O R υCC, υCO, L υCO sym, MeOH υCO |
| 939 | M | 958 | 942 | R υCC, υCO asym, MeOH υCC, $\delta CH_2$ |
| 892 | W | | | R υCC, υCO sym, δCH, MeOH υCC, $\delta CH_2$ |
| 871 | M | 883 | 868 | R υCC, υCO sym, L δC1OC4 |
| 805 | M | 834 | 820 | R δOC1C2, L δC1OC4 |

Vibrations localized to the glycosidic linkage, cyclic (ring) fragment or exocyclic C6-OH are preceded by symbols "L", "R" or "MeOH", respectively. Stretching and bending vibrations are denoted υ and δ, respectively, symmetric and asymmetric vibrations by "sym" and "asym". Three mannan bands are not assigned any simulated bands due to poor convergence in this spectral interval.

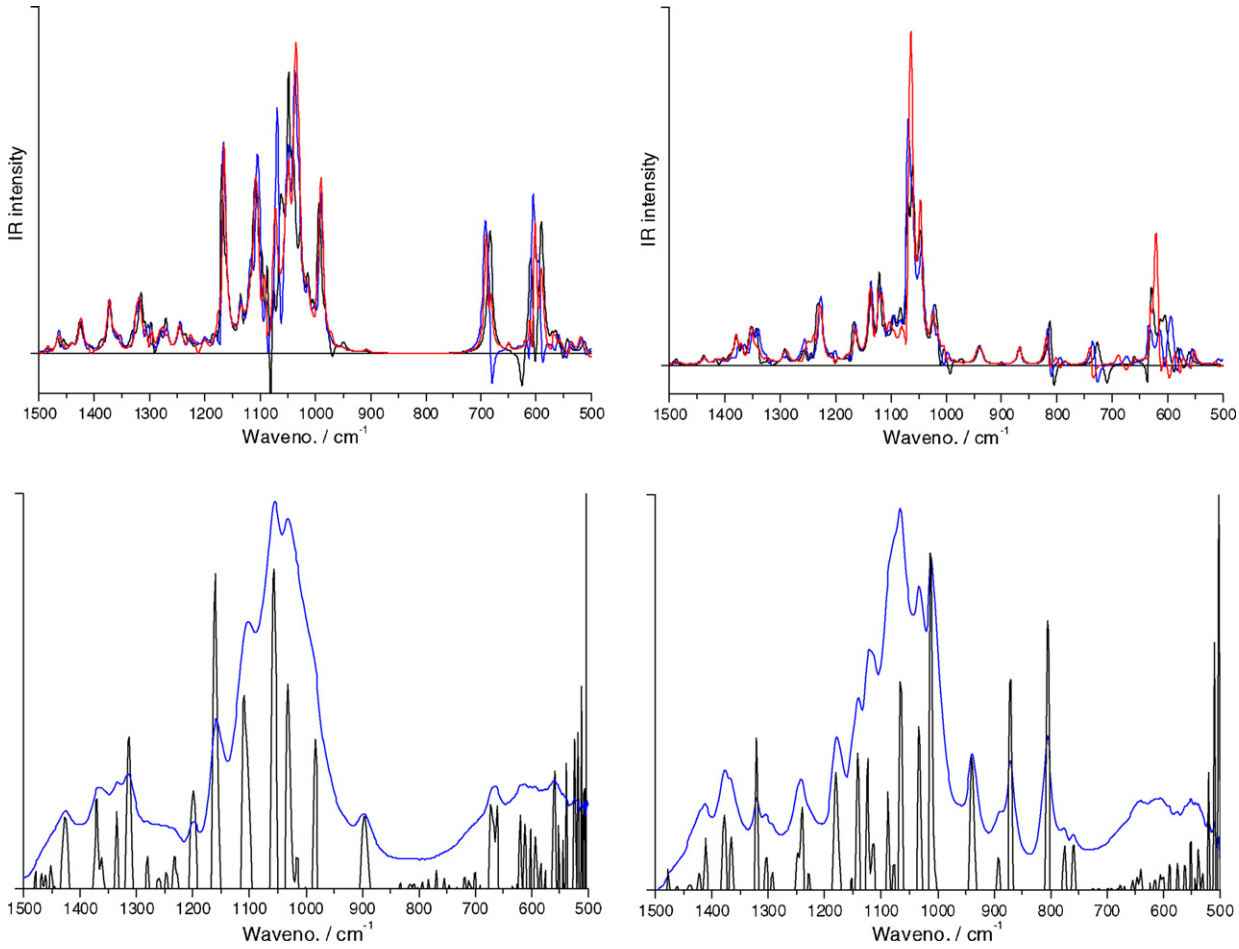


**Fig. 2.** Predicted incremental IR spectra (top) and observed ATR-IR spectra (bottom, with sign-inversed and scaled 2der spectra superimposed) of cellulose (left side) and mannan (right side). The predicted spectra are shown for the DP = 2–3 (in black), the DP = 3–4 (in blue) and DP = 4–5 (in red) increment, respectively. (For interpretation of the references to color in this figure legend, the reader is referred to the web version of the article.)
The predicted spectra of cellulose are adopted from Barsberg (2010).

bands, are caused by combinations of vibration types (e.g. $\upsilon$CC, $\upsilon$CO, $\delta CH_2$, etc.) not found for cellulose and *vice versa*. Another interesting example is the cellulose 896 $cm^{-1}$ band, which is caused predominantly by (concerted) $CH_2$ wagging of the MeOH group. Contrary to this the mannan band at 892 $cm^{-1}$ is caused by a complex combination of several vibration types, which weakens its intrinsic IR activity compared to that of the cellulose 896 $cm^{-1}$ band. The nature of the predicted mannan vibrations show that actually none of these correspond to this cellulose band.

Within the higher wave number region >900 $cm^{-1}$ the IR spectra have more similarities and some of the cellulose and mannan vibrations are qualitatively identical. Thus the predictions confirm that the mannan bands observed at 1011, 1033, and 1180 $cm^{-1}$ correspond to the cellulose bands at 1032, 1058, and 1161 $cm^{-1}$, respectively (see Table 1).

### 4.3. Sugar composition

The composition of the sieved PKC material was on a dry matter basis: glucose 8.0 ± 0.5%, xylose 1.8 ± 0.2%, arabinose 1.4 ± 0.1%, galactose 2.3 ± 0.1%, mannose 41.7 ± 1.9%, klason lignin 10.2 ± 1.3%, protein 16.8 ± 0.3% and ash 4.4 ± 0.1% (sugars reported as anhydrous form), sum total = 86.6%. In addition, PKC contains 5–10% residual oil (not measured), which could be observed floating on top of the slurry after the hydrolysis stage. Of the total composition, 55% is sugars of which mannose makes up about 76%. Thus the PKC material has a relatively low (6%) α-D-galactopyranose (galactose) substitution of the mannan, and previously determined low levels of (4-O-methyl)-glucurono and arabinoxylans are consistent with the present results. It must be pointed out that both the sugars and protein content can vary according to the source of PKC.

PKC was used as feedstock for bioethanol production. In the tested setup, the materials were first pre-hydrolyzed for 24 h at 50 °C after which the temperature was lowered to 32 °C and fermented for 168 h. After pre-hydrolysis the yield of glucose and mannose in the slurry was 25.4 ± 0.3 g (2.3% of original PKC) and 198.5 ± 2.5 g (18%) per kg of original dry PKC, respectively. The amount of mannose was about 88% of the total sugars released during the pre-hydrolysis step, and for the two main components it is noted that nearly 1/2 of the available mannose is released whereas only ~¼ of the glucose is released. The SSF step produced 165 g ethanol per kg PKC, which corresponds to 60% of the mannose and glucose being fermented. The removal of most of the mannan and cellulose in the PKC after the SSF step increased the protein content of the solid residue (dry matter) by 70% to 28.5 ± 0.2%.

In summary we correct the composition values of sample types H and HSSF by a factor (86.6%/sum total%) > 1 to reach the 100% level of the sieved PKC. Since the focus is on cellulose and mannan not all values were analyzed for. The Xyl, Ara and Gal are assumed zero (in reality very small), and lignin, protein and ash values assumed unchanged by the H and HSSF steps. The final HSSF step leaves 40% of the original (41.7 + 8%) mannose and glucose in the sample for which their sum is thus reduced to 20%. The individual numbers are not known but assuming the glucose value to be reduced further

from H → HSSF by ~¼ these are estimated as ~4–5% (glu) and 15–16% (man). The expected error margins of these assumptions have small impact on the trends shown by the following data.

The *corrected* compositions in terms of the dominant components thus changes as (original sieved PKC → H → HSSF): glucose: 8.0 → 8.1 → 7–8%, mannose: 41.7 → 34.1 → 25–27%, lignin: 10.2 → 14.4 → 17.2%, protein: 16.8 → 23.8 → 28.3%, ash: 4.4 → 6.2 → 7.4%. Thus the relatively large removal of mannan in effect up-concentrates other components as accounted for by the correction factor. For cellulose this appears to balance with its removal such that its effective concentration in the remaining sample is practically constant.

### 4.4. ATR-IR spectra of PKC samples

Since the ATR correction has little effect on the band positions the PKC sample spectra were not corrected. The spectra were normalized at 700 $cm^{-1}$ where they are devoid of distinct IR bands.

In the 600–1200 $cm^{-1}$ interval a decrease of several distinct bands can be observed, and the 1200–1700 $cm^{-1}$ interval exhibits a general increase of several bands some of which are quite broad. In addition the distinct band at 1740 $cm^{-1}$ is nearly removed after the HSSF treatment. The spectra show clearly the degradation and removal of mannan through the relatively large decrease of the three characteristic mannan bands in the 800–950 $cm^{-1}$ interval. Concomitant with the removal of mannan a relative increase in surface layer concentration of those components, e.g. proteins, not affected by the treatments is observed. Thus the relative increase of band intensity in the 1500–1650 $cm^{-1}$ interval can be assigned the strongest protein Amide I and II bands at ~1650 and 1550 $cm^{-1}$, respectively. Although the gross effects of the treatments are evident from Fig. 3 – and appear to follow the trend of the *corrected* composition values (see Section 4.3) – more details are revealed by the 2der spectra depicted in Fig. 4.

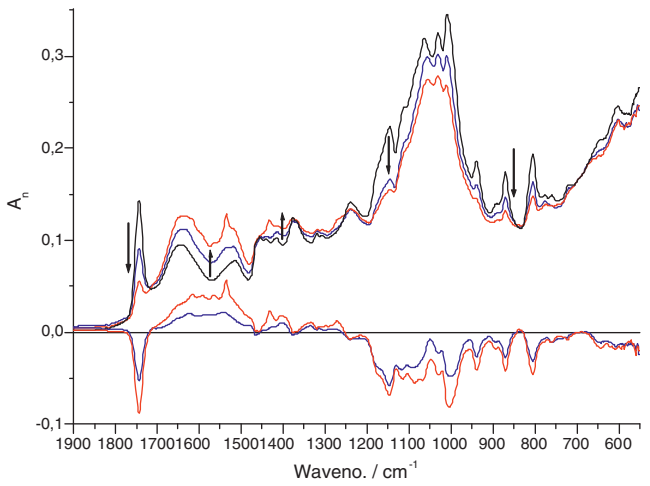


**Fig. 3.** Normalized ATR-IR average spectrum of original (in black line), H (blue) and HSSF (red) solid residue samples, and the corresponding difference spectra relative to the original for the H (blue) and HSSF samples (red). The arrows show direction of spectral changes. (For interpretation of the references to color in this figure legend, the reader is referred to the web version of the article.)

The second derivative provides resolution enhancement of overlapping narrow bands and may enhance small narrow bands from broader features, e.g. the lignin 1515 $cm^{-1}$ band from broad protein absorption. It should be noted that for quantitative work the 2der procedure does not conserve relative IR band areas for which other methods must be used, e.g. Fourier de-convolution. The figure shows the 2der of all (normalized) spectra, i.e. the ten control

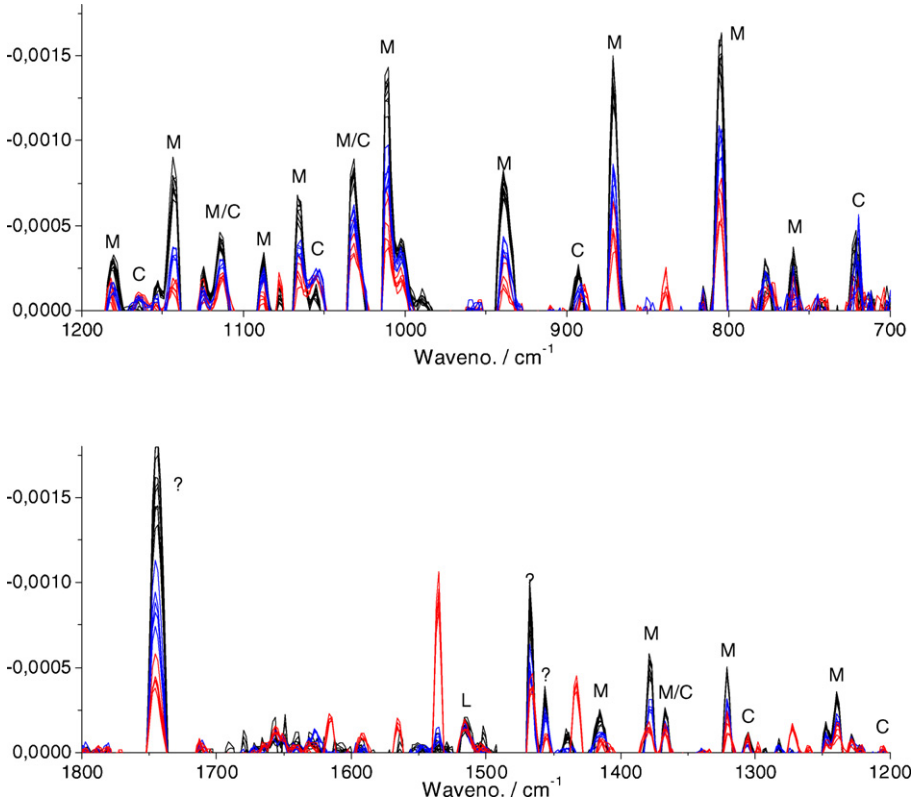


**Fig. 4.** Second derivative of ATR-IR spectra of original (control, black lines), H (blue lines) and HSSF samples (red lines). Bands are assigned to mannan (M), cellulose (C) or lignin (L). Bands denoted M/C occur where mannan and cellulose have overlapping bands. (For interpretation of the references to color in this figure legend, the reader is referred to the web version of the article.)

samples and five H and HSSF treated sample spectra. They confirm the significant decrease of all mannan associated bands for the H and HSSF samples. Changes of cellulose associated bands are less evident, and even the strongest cellulose bands appear weak for the PKC samples. These are the five bands positioned at 989, 1029, 1055, 1110, and 1164 $cm^{-1}$. The 1029 and 1110 $cm^{-1}$ bands occur at the same position as mannan bands, but the remaining three bands appear resolved or partially resolved from mannan bands. They show no consistent change in overall strength in accordance with a practically unchanged corrected glucose value of ~8%. The 2der 1055 $cm^{-1}$ band is slightly increased by both H and HSSF treatments, whereas a small decrease is observed for the 989, 893 and 721 $cm^{-1}$ bands.

For nearly all bands no positional shift >1 $cm^{-1}$ is observed as function of treatment. However, the 893 $cm^{-1}$ cellulose band shows a clear positional negative shift as function of the treatment severity from $892.8 \pm 0.2$ $cm^{-1}$ (original PKC) to $892 \pm 1$ $cm^{-1}$ (H) to $889 \pm 1$ $cm^{-1}$ (HSSF). Also the mannan 1180 $cm^{-1}$ band shows a shift, which is positive, and most marked going from the H to the HSSF treatment for which its position is 1182 $cm^{-1}$.

The lignin component band at 1515 $cm^{-1}$ is not affected by the treatments. According to the sugar composition analysis the lignin and protein concentration should both increase significantly. This indicates that lignin is actually removed possibly along with closely associated xylan extracted during treatments. Close to this band two sharp bands (of less certain origin) at 1456 and 1467 $cm^{-1}$ are both affected by the treatments. Some impurity bands – induced by the SSF step of the treatments – are observed both in the original spectra (Fig. 3) and in the 2der spectra, where the strongest appear at 1272, 1433 and 1535 $cm^{-1}$.

## 5. Discussion

Figs. 2 and 4 provide strong evidence that all major features in the 2der spectra, positioned at wave numbers <ca. 1400 $cm^{-1}$ are indeed caused by mannan, and that weaker features are predominantly associated with cellulose. The sugar analysis shows that other hemicelluloses are present in very low concentration. Thus their $\upsilon$CO backbone ring and linkage vibrations, which dominate their IR spectrum at ca. 1000–1100 $cm^{-1}$, will (assuming roughly the same *intrinsic* intensities) be correspondingly weaker relative to those of cellulose. Previous work on FT-IR spectroscopy of hemicelluloses report the dominant band of glucuronoxylan and arabinoxylan at 1047 $cm^{-1}$, i.e. 10 $cm^{-1}$ below the 1057 $cm^{-1}$ cellulose band (Kacuráková, Capek, Sasinikova, Wellner, & Ebringerová, 2000; Kacuráková et al., 1999; Robert, Marquis, Barron, Guillon, & Saulnier, 2005). The 2der spectra depict no observable band at this position, which is sufficiently separated from that of the cellulose band to enable resolution of a possible xylan band. Bands associated with such structures are therefore (for the samples and instrumental settings used) below the detection limit in the 2der spectra. This may not be the case in the original spectra but in these they cannot be resolved from other polysaccharide bands.

Thus the bands in the 2der spectra which report on the largest structural changes are caused by mannan as well as by a structure with a strong band at 1744 $cm^{-1}$. The significant decrease of this band follows that of the mannan bands, and its position suggests that it is caused by a carbonyl containing structure, e.g. acetyl esters, closely associated with mannan although it cannot be ruled out that it is associated with extracted palm oil. It may conceivable substitute the mannan backbone chain, without much perturbation of its IR signatures or it may substitute another hemicellulose, e.g. xylan, so as to dominate its IR signature. The two bands at 1456 and 1467 $cm^{-1}$ appear to be too strong to be assigned mannan (or cellulose), which have very weak 2der peaks in this part of the spectrum. The fact that they are both reduced by the HSSF treatment, whereas the 1515 $cm^{-1}$ lignin band is not, suggests that they do not originate from lignin. Since they have relatively significant strengths they may be associated with galacto substitution of the mannan chain. The IR signatures of such substructures are of course *not* revealed by the unsubstituted linear chain mannan modelling or the mannan reference sample.

Although not all observed bands can be assigned they reveal apparently two different kinetic traits, i.e. a relatively fast mannan degradation concomitant with none or a slow degradation of cellulose and lignin. Lignin is not hydrolyzed (it is not a substrate for the enzymes used) but appears to be partially co-extracted and removed with hemicellulose. In accordance with the corrected sugar composition values the spectra do not report on the absolute removal of cell wall components but on the change of their *relative* concentrations within the probed sample layer. Since mannan is degraded to a much larger extent, all other components are (depending on their degree of degradation) being up-concentrated in the residue. This effect counteracts the observation of relatively small decreases of the mass of some components in their normalized band intensities.

In spite of these difficulties interesting band position observations can still be made, namely that the cellulose 896 $cm^{-1}$ (893 $cm^{-1}$ in PKC) and mannan 1180 $cm^{-1}$ bands shift positions by −4 $cm^{-1}$ and +2 $cm^{-1}$, respectively.

For the cellulose band this indicates that the *environment of the cellulose C6-OH group changes*. Diffraction experiments on cellulose Iβ has determined its molecular structure to better than 1 Å resolution and elucidated its hydrogen (H) bonding system (Nishiyama et al., 2002). H bonds from C3-OH to O5 along the chain are consistently present, whereas the C6-OH and C2-OH form two mutually exclusive H bonding systems. These two systems are abbreviated H bonding network A (NWA) and H bonding network B (NWB), respectively. In previous theoretical work the reduction of the intensity of the 896 $cm^{-1}$ band was suggested to arise from a relatively larger occurrence of NWB in which the C6-OH hydrogen bonds *intra*-molecular *versus inter*-molecular in NWA (Barsberg, 2010). This work also indicated that the frequency of this vibration is sensitive to the environment.

The relative energy and population of these two C6-OH conformations are most likely affected by close association of cellulose to mannan since cellulose C6-OH groups may engage in intermolecular H bonds – as donor (NWA) *or* acceptor (NWB) – to a proximate mannan chain. The *highly localized* $C6H_2$ vibration of this group is strongly coupled with the specific environment (H bonding) of its –OH group. In relation to the present work we suggest that it "senses" the degradation of closely associated cellulose or mannan chains. When H bonding to such chains is no longer possible the relative free energy of the two networks will change and their relative occurrence change provided there are no significant kinetic barriers. The intensity and position of the 896 $cm^{-1}$ band will accordingly change.

The mannan band observed at 1180 $cm^{-1}$ is caused by (predominantly) the antisymmetric $\upsilon$COC glycosidic linkage vibration, i.e. positioned ca. +20 $cm^{-1}$ relative to the position of the analogous cellulose band. This assignment follows from the DFT simulation of the mannan IR spectrum. The predictions based on the individual mannan oligomer models show that increasing DP (degree of polymerization) leads to a lower frequency of the (most IR active) normal modes corresponding to this vibration. From DP = 2 to DP = 5 (the largest oligomer model) the predicted unscaled frequency shifts from 1195 to 1186 $cm^{-1}$, respectively. This suggests that the exact position of the mannan 1180 $cm^{-1}$ band may indicate the overall DP of mannan. The position appears to be less affected during pre-hydrolysis than SSF, where most of the +2 $cm^{-1}$ shift occurs. The simulation results indicate that when the DP is sufficiently low,

approaching oligomer sizes <10, this shift becomes noticeable. In extension of this supposition the analogy suggests itself that the 1161 $cm^{-1}$ band of cellulose also reports on the overall DP of cellulose. The strength of this (2der) band is, however, too low for the samples analyzed to enable any conclusions to be drawn.

Whereas this positional shift of the L $\upsilon$CO asym vibration is predicted for isolated weakly interacting chains it cannot be ruled out that other effects may also cause a shift. The polysaccharide chains are not isolated in real samples, and their vibrations may couple with adjacent more or less loosely packed chains or they may couple with a changing environment polarity all of which could also change with polysaccharide degradation.

## 6. Conclusions

The present work has demonstrated the potential strength of ATR-IR spectroscopy for *in situ* analysis of the macromolecular nature and constitution of plant cell walls, and the changes these may suffer. A convincing and detailed support for the analysis is provided by spectra of reference samples and DFT modelling of their vibrational signatures. For practical reasons the modelling was limited to consider only the main polysaccharide constituents, i.e. simple homogeneous systems of poly(gluco- and mannopyranose) as cellulose and mannan models, respectively. A more detailed account of the change of PKC state during enzymatic hydrolysis would also address the minor polysaccharide components and substituents, e.g. galacto substitution of mannan. The IR bands of such structures are close to or below detection limit in the present work.

We have also shown a potential of analyzing the positional shifts of IR bands. For the samples used in the present work this was exemplified by what may be termed the 896 $cm^{-1}$ "environment sensor band" of cellulose, and the 1180 $cm^{-1}$ band of mannan.

For the two main PKC polysaccharides mannan and cellulose we have exemplified the importance of DFT for a detailed understanding of FT-IR analysis results, namely the identification and assignment of their IR signatures. This is a *general prerequisite* for a possible quantitative use of FT-IR in respect to any cell wall polymer component. In principle more information can be extracted from band intensities and positional shifts but it is not a simple task as these can be the net result of various different effects.

## References


Aspinall, G. O. (1970). Mannans, galactomannans and glucomannas. In G. O. Aspinall (Ed.), *Polysaccharides* (pp. 85–94). Oxford: Pergamon Press Ltd.

Barsberg, S. (2010). Prediction of vibrational spectra of polysaccharides-simulated IR spectrum of cellulose based on Density Functional Theory (DFT). *Journal of Physical Chemistry B, 114*(36), 11703–11708.

Berepubo, N. A., Mepba, H. D., Agboola, O. J., & Onianwah, R. I. (1995). Inclusion rate and true metabolizable energy of palm kernal cake in broiler chicken diets in a huamid tropical environment. *Journal of Applied Animal Research*, *7*(1), 27–34.

Chanzy, H., Perez, S., Miller, D. P., Paradossi, G., & Winter, W. T. (1987). An electron-diffraction study of mannan. 1. Crystal and molecular-structure. *Macromolecules*, *20*(10), 2407–2413.

da Luz, B. R. (2006). Attenuated total reflectance spectroscopy of plant leaves: A tool for ecological and botanical studies. *New Phytologist*, *172*(2), 305–318.

Düsterhöft, E. M., Bonte, A. W., & Voragen, A. G. J. (1993). Solubilization of nonstarch polysaccharides from oilseed meals by polysaccharide-degrading enzymes. *Journal of the Science of Food and Agriculture*, *63*(2), 211–220.

Düsterhöft, E. M., Posthumus, M. A., & Voragen, A. G. J. (1992). Nonstarch polysaccharides from sunflower (*Helianthus-Annuus*) meal and palm-kernel (*Elaeis-Guineensis*) meal investigation of the structure of major polysaccharides. *Journal of the Science of Food and Agriculture*, *59*(2), 151–160.

Gaussian. (2004). *Gaussian 03W, Revision D.01*. Wallingford, CT: Gaussian, Inc.

Goormaghtigh, E., Raussens, V., & Ruysschaert, J. M. (1999). Attenuated total reflection infrared spectroscopy of proteins and lipids in biological membranes. *Biochimica et Biophysica Acta-Reviews on Biomembranes*, *1422*(2), 105–185.

Huang, Z., Cooper, P., Wang, X. D., Wang, X. M., Zhang, Y. L., & Casilla, R. (2010). Effects of conditioning exposure on the pH distribution near adhesive wood bond lines. *Wood and Fiber Science*, *42*(2), 219–228.

Joo, J. H., & Yun, J. W. (2005). Structural and molecular characterization of extracellular polysaccharides produced by a new fungal strain, *Trichoderma erinaceum* DG-312. *Journal of Microbiology and Biotechnology*, *15*(6), 1250–1257.

Jørgensen, H., Sanadi, A. R., Felby, C., Lange, N. E. K., Fisher, M., & Ernst, S. (2009). Production of ethanol and feed by high dry matter hydrolysis and fermentation of palm kernel press cake. *Applied Biochemistry and Biotechnology*.

Kacuráková, M., Capek, P., Sasinikova, V., Wellner, N., & Ebringerová, A. (2000). FT-IR study of plant cell wall model compounds: Pectic polysaccharides and hemicelluloses. *Carbohydrate Polymers*, *43*(2), 195–203.

Kacuráková, M., Wellner, N., Ebringerová, A., Hromádková, Z., Wilson, R. H., & Belton, P. S. (1999). Characterisation of xylan-type polysaccharides and associated cell wall components by FT-IR and FT-Raman spectroscopies. *Food Hydrocolloids*, *13*(1), 35–41.

Kaparaju, P., & Felby, C. (2010). Characterization of lignin during oxidative and hydrothermal pre-treatment processes of wheat straw and corn stover. *Bioresource Technology*, *101*(9), 3175–3181.

Kasarova, S. N., Sultanova, N. G., Ivanov, C. D., & Nikolov, I. D. (2007). Analysis of the dispersion of optical plastic materials. *Optical Materials*, *29*(11), 1481–1490.

Kath, F., & Kulicke, W. M. (1999). Polymer analytical characterization of glucan and mannan from yeast *Saccharomyces cerevisiae*. *Angewandte Makromolekulare Chemie*, *268*, 69–80.

Kirov, K. R., & Assender, H. E. (2005). Quantitative ATR-IR analysis of anisotropic polymer films: Surface structure of commercial PET. *Macromolecules*, *38*(22), 9258–9265.

Knudsen, K. E. B. (1997). Carbohydrate and lignin contents of plant materials used in animal feeding. *Animal Feed Science and Technology*, *67*(4), 319–338.

Kristensen, J. B., Felby, C., & Jørgensen, H. (2009). Determining yields in high solids enzymatic hydrolysis of biomass. *Applied Biochemistry and Biotechnology*, *156*(1–3), 127–132.

Lin, W. D., & Li, Z. J. (2010). Detection and quantification of trace organic contaminants in water using the FT-IR-attenuated total reflectance technique. *Analytical Chemistry*, *82*(2), 505–515.

Nishiyama, Y., Langan, P., & Chanzy, H. (2002). Crystal structure and hydrogen-bonding system in cellulose 1 beta from synchrotron X-ray and neutron fiber diffraction. *Journal of the American Chemical Society*, *124*(31), 9074–9082.

O'Mara, F. P., Mulligan, F. J., Cronin, E. J., Rath, M., & Caffrey, P. J. (1999). The nutritive value of palm kernel meal measured in vivo and using rumen fluid and enzymatic techniques. *Livestock Production Science*, *60*(2–3), 305–316.

Oberg, K. A., & Fink, A. L. (1998). A new attenuated total reflectance Fourier transform infrared spectroscopy method for the study of proteins in solution. *Analytical Biochemistry*, *256*(1), 92–106.

Palm Oil World. (2009). *Global trade*. http://www.palmoilworld.org/Globaltrade.htm

Ramachandran, S., Singh, S. K., Larroche, C., Soccol, C. R., & Pandey, A. (2007). Oil cakes and their biotechnological applications – A review. *Bioresource Technology*, *98*(10), 2000–2009.

Robert, P., Marquis, M., Barron, C., Guillon, F., & Saulnier, L. (2005). FT-IR investigation of cell wall polysaccharides from cereal grains. Arabinoxylan infrared assignment. *Journal of Agricultural and Food Chemistry*, *53*(18), 7014–7018.

Sluiter, A., Hames, B., Ruiz, R., Scarlata, C., Sluiter, J., Templeton, D., et al. (2006). *Determination of structural carbohydrates and lignin in biomass*. Golden, CO, USA: National Renewable Energy Laboratory. http://devafdc.nrel.gov/pdfs/9572.pdf

Sundu, B., Kumar, A., & Dingle, J. (2006). Palm kernel meal in broiler diets: Effect on chicken performance and health. *Worlds Poultry Science Journal*, *62*(2), 316–325.

USDA Foreign Agricultural Service. (2009). *Palm oil: World supply and distribution*. http://www.fas.usda.gov/psdonline/psdreport.aspx?hidReportRetrievalName=BVS&hidReportRetrievalID=710&hidReportRetrievalTemplateID=8

Yu, Z. J., Jiang, Y. Q., Zou, W. W., Duan, J. J., & Xiong, X. P. (2009). Preparation and characterization of cellulose and konjac glucomannan blend film from ionic liquid. *Journal of Polymer Science Part B-Polymer Physics*, *47*(17), 1686–1694.

Yui, T., Miyawaki, K., Yada, M., & Ogawa, K. (1997). An evaluation of crystal structure of mannan I by X-ray powder diffraction and molecular mechanics studies. *International Journal of Biological Macromolecules*, *21*(3), 243–250.